Biointerface Research in Applied Chemistry
Open-Access Journal (ISSN: 2069-5837)

Article
Volume 16, Issue 4, 2026, 106
https://doi.org/10.33263/BRIAC164.106

Is Doped BN-based Nanomaterial a Capable Surface for Drug Delivery through COVID-19?

Fatemeh Mollaamin [1,*]

[1] Department of Biomedical Engineering, Faculty of Engineering and Architecture, Kastamonu University, Kastamonu, Turkey
* Correspondence: fmollaamin@kastamonu.edu.tr;

Received: 27.03.2026; Accepted: 29.05.2026; Published: 15.08.2026

Abstract: In this work, chloroquine (CLQ) has been evaluated for its inhibition of coronavirus using trapping on the boron nitride nanocage (B4N10) functionalized with some atoms as a drug delivery procedure, owing to the direct electron transfer principle, as illustrated by the quantum mechanics method of molecular modeling. In fact, the theoretical approach using CAM-B3LYP/6-311+G (d,p) explains how B_4N_{10} binds the CLQ drug through electronic-state density, nuclear quadrupole resonance, nuclear magnetic resonance, and thermodynamic properties. In the end, the results showed that using B_4N_{10} modified with aluminum, carbon, and silicon for adsorbing the CLQ drug to form "B_4AlN_{10}–CLQ, B_4CN_{10}–CLQ, and B_4SiN_{10}–CLQ" could yield a promising drug-delivery formulation. This can be supported by quantum-mechanical calculations based on the physical and chemical properties shown in PDOS, NMR, NQR, and IR spectra. Here, we used network pharmacology, metabolite analysis, and molecular simulation to elucidate the biochemical basis of the health-promoting effects of the CLQ drug via B4N10-mediated drug delivery.

Keywords: B_4XN_{10} (X=Al/C/Si); drug delivery; CLQ; COVID–19; quantum DFT.

1. Introduction

The arrival of a recent coronavirus, known as the severe acute respiratory syndrome coronavirus 2 (SARS–CoV–2), has involved a pandemic of Coronavirus Disease of 2019 (COVID–19) [1,2]. Following its precedent, a reported case in Wuhan, China, in December 2019, recent studies by medical professionals and scientists have supported some ideas about the virus's pathogenesis and nature [3]. The intensity of the COVID-19 pandemic has waned since the beginning of 2022, in parallel with a significantly reduced risk for disease progression and death due to widespread vaccination, hybrid immunity, and the intrinsically low virulence of the Omicron subvariants [4]. The use of early therapies (antiviral monoclonal antibodies and small molecules) has been approved for preventing disease progression and hospitalizations among high-risk outpatients with comorbidities [5]. Gottlieb *et al*. investigated the early treatment of COVID-19 outpatients with oral antivirals or short daily infusions, a strategy that helped turn the tide of the pandemic by reducing hospital admissions and mortality [6]. Furthermore, Kim *et al*. have indicated that, while treatment options for patients with severe disease requiring hospitalization are now available, with corticosteroids emerging as the treatment of choice for critically ill patients, interventions that can be administered early during

infection to prevent disease progression and longer-term complications are urgently needed [7]. There is not a certain therapy or vaccine receivable to battle versus SARS–CoV–2 [8]. Lately, antibodies have been almost all created in human cells and transformed animal cells, which are programs with many tools that are very difficult to run [9,10]. In addition, SARS-CoV-2 is a current major challenge for researchers, and they are still working on the development of antiviral drugs against SARS-CoV-2 [11–13]. Currently, researchers and scientists are working on the development of a drug against COVID-19 in the following ways: the prevention of self-assembly (structural proteins), viral replication (Nsps), viral entry, and the blocking of the signaling pathways required for viral infection [14–16].

Chloroquine, with the formula $C_{18}H_{26}ClN_3$, has antiviral and anti-inflammatory properties and has been used for the treatment of MERS–CoV, Zika virus, enterovirus EV–A71, OC43, influenza A H5N1, SARS–CoV, and SARS–CoV–2 infections [17,18].

Recently, several studies have investigated the potential benefits of chloroquine or its derivative, hydroxychloroquine, an inexpensive antimalarial medication that has been used for years in COVID-19 therapy [19, 20].

Daolin *et al*. have shown that chloroquine, with a dual function in antiviral immunity, can be critical to consider for introducing in the COVID-19 cure [21].

There is a need to enhance the bioavailability and operational interval of a medication to achieve therapeutic outcomes. Drug delivery approaches can alter a medication's pharmacokinetics and quality by providing diverse components, drug delivery systems, and medical devices [22–25].

Among nanoparticles, boron nitride (BN) nanomaterials have shown excellent physical and chemical properties and a wide range of applications in drug delivery systems [26]. In this work, the focus was on the CLQ drug attached to functionalized B4N10_NC with Al, C, and Si atoms, towards the formation of B4AlN10–CLQ, B4CN10–CLQ, and B4SiN10–CLQ complexes for the treatment of COVID–19 (Figure 1).

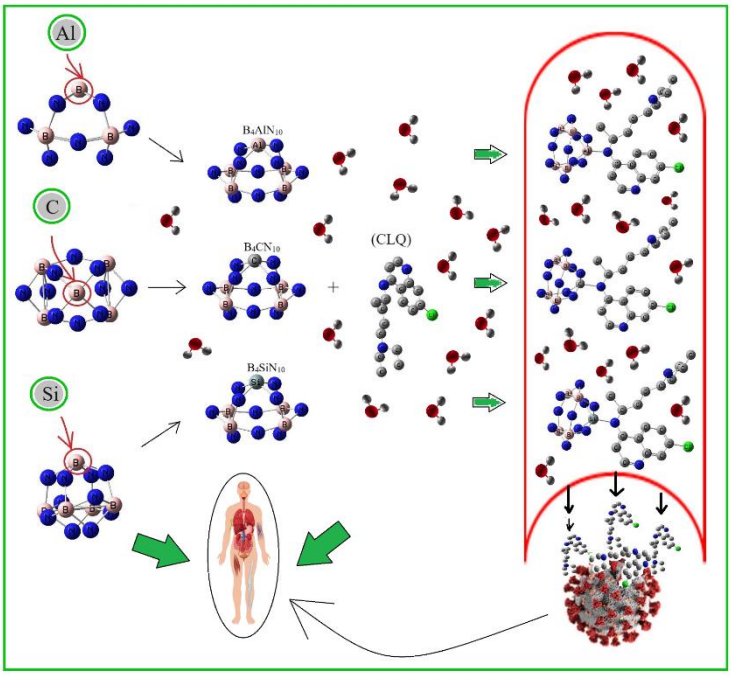

Figure1. Adsorption of chloroquine (CLQ) by functionalized B_4N_{10} with Al, C, and Si atoms towards formation of B_4AlN_{10}–CLQ, B_4CN_{10}–CLQ, and B_4SiN_{10}–CLQ complexes.

The COVID-19 pandemic, driven by the constantly changing SARS-CoV-2 virus, has kept global health systems on high alert. With new virus strains appearing regularly, many of which spread more easily and can escape immune defenses, worries about how well current vaccines and treatments work have grown. As resistance to antiviral drugs and monoclonal antibodies becomes more common, doctors are looking at combining different treatments and developing new, more powerful antibodies that can fight a wider range of virus variants [27].

2. Theoretical Background, Materials, and Methods

The theoretical method of density functional theory (DFT) is one of the most widely used approximations of Hohenberg, Kohn, and Sham, which enables the theoretical investigation of material properties [28]. The DFT approach provides a beneficial level for estimating chemical systems [29].

In this work, the structures of CLQ drug adsorbed on the B_4XN_{10} (X=Al/C/Si) were minimized at the skeleton of the DFT approach, accompanied by the three-parameter Becke's exchange [30] and Lee–Yang–Parr's correlation non-local functional [31], introduced as B3LYP level. The calculations used the basis sets of LANL2DZ and 6–311+G (d,p) with multiplicity of +1 and convergence on RMS density matrix=1.00D-08 and convergence on MAX density matrix=1.00D-06. In fact, molecular modeling techniques are used to describe the process of interaction between CLQ drug and B_4XN_{10} (X=Al/C/Si) towards formation of B_4AlN_{10}–CLQ, B_4CN_{10}–CLQ, B_4SiN_{10}–CLQ complexes as the drug delivery system for treatment of Covid-19 disease (Figure 1).

In this research, the Onsager pattern was carried out, which was extended by Frisch, Wong, and Wiberg by applying spherical cavities [32]. This model provides a less accurate explanation of the solute/solvent interface, but it can lighten the assessment of energy derivatives during optimization and frequency analysis. Furthermore, Cramer and Truhlar developed this model at the dipole level [33]. As a matter of fact, a cavity should have a physical impression, as in the Onsager design, and a mathematical susceptibility, as is frequently the case in other definitions of solvent influences [32]. So, the cavity must maintain the solvent and its neighbors as the greatest possible section of the solute charge diffusion [34].

The CNT compound is discussed in drug-delivery programs that might be implemented using a variety of biomaterials containing DNA, proteins, and antibodies. This provides clearance for the purpose of assigning special cells, tissues, and organs. These substances might lightly interpenetrate cells, releasing medications directly to the nucleus or cytoplasm. Drug-releasing platforms enhance the pharmacological and therapeutic profile and influence of the medication, and reduce the occurrence of off-target effects [35].

In fact, a mass of quantum mechanical techniques can accomplish discovering certain properties of physico-chemical specifications extracted from a minimized frame of CLQ drug attached to B_4XN_{10} (X=Al/C/Si), consisting of density of electrical states, electric potential, Bader charge distribution, vibrational computations, and nuclear magnetic resonance analysis, owing to running a drug delivery model using the Gaussian 16 revision C.01 program [36]. In addition, the gauge-including atomic orbitals (GIAO) method has been used to assess gauge-origin issues in the measurement of nuclear magnetic shielding for [B_4XN_{10}–CLQ (X=Al/C/Si)] complexes using DFT.

3. Results and Discussion

3.1. PDOS study.

The electronic structures of the CLQ drug attached to the B_4XN_{10} (X=Al/C/Si) nanocage were evaluated to explain the interfacial electronic parameters using quantum methods.

Figure 2 (a–d) introduces the projected density of states (PDOS) of the CLQ drug, B_4AlN_{10}, B_4CN_{10}, and B_4SiN_{10}, respectively. It is obvious from the figure that after adsorption of the CLQ drug on the B_4XN_{10} (X=Al/C/Si), there is a significant contribution of *p*-orbitals of Al, C, Si, N, and Cl atoms in the unoccupied stage. Population analysis and PDOS indicate that C, N, and Cl atoms of CLQ remain in linkage with B_4XN_{10}(X=Al/C/Si), and they can grab more electrons from other elements. So, the graph of PDOS reveals that the *p* states of the adsorption of C, N, and Cl atoms on the B_4XN_{10}–C(X=Al/C/Si) are significant through the conduction band (Figure 2a–d). Furthermore, the existence of covalent features for the [B_4XN_{10}–CLQ (X=Al/C/Si)] complex has shown the equal energy content and configuration of the PDOS for the *p* orbitals of Al, C, Si, N, and Cl atoms (Figure 2a–b).

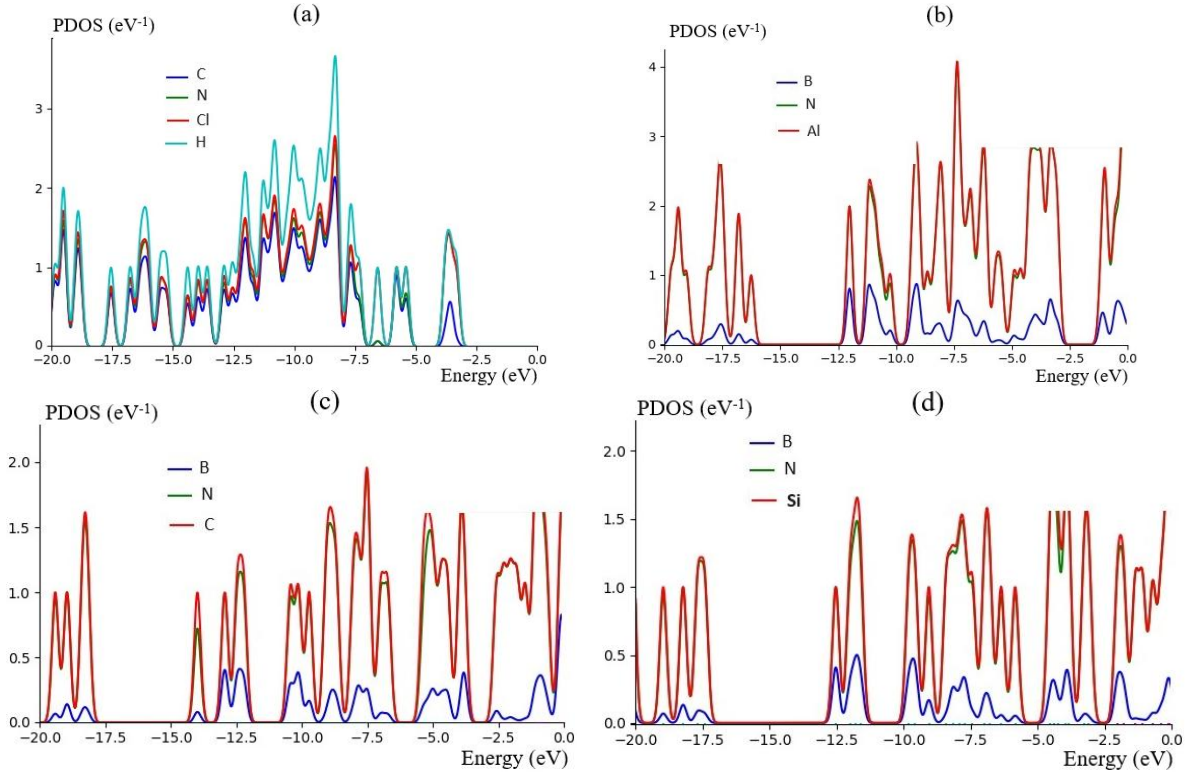

Figure 2. Electronic properties of Partial Density of States (PDOS) for **(a)** CLQ drug adsorbed on **(b)** B_4AlN_{10}–CLQ; **(c)** B_4CN_{10}–CLQ; **(d)** B_4SiN_{10}–CLQ.

Figure2a–d shows that the CLQ drug states adsorbed onto B_4XN_{10}(X=Al/C/Si) complexes have more contribution at the middle of the conduction band between –5eV to –15eV, while contribution of C, N, Cl states in CLQ drug are expanded and close together (Figure 2a), and Al states in B_4AlN_{10} (Figure 2b), C in B_4CN_{10} (Figure 2c) and Si in B_4SiN_{10} (Figure 2d) approximately have the most contributions.

As a matter of fact, the aforementioned consequences indicate that the principal complex and a certain degree of covalent character can narrow the direct band gap of the CLQ drug when absorbed on the B_4XN_{10} (X=Al/C/Si) complexes.

3.2. Spectroscopy of NMR.

The nuclear magnetic resonance (NMR) information of shielding tensors (ppm) containing isotropic (σ_{iso}) and anisotropic (σ_{aniso}) for CLQ drug linked to B_4XN_{10} (X=Al/C/Si) complexes was computed (Table 1). The results obtained demonstrate the "SCF/GIAO" magnetic shielding tensor for Al, C, Si, N, and Cl atoms, revealing the active zone of the CLQ material as a potential therapeutic agent for viral disease treatment. The measurements were run at the "B3LYP/6–311+G (d, p)" level of theory using the Gaussian 16 revision C.01 program [28] and were reported in Table 1.

Table 1. Data of nuclear magnetic resonance (NMR) tensors (ppm) for CLQ drug attached to B_4AlN_{10}, B_4CN_{10}, and $B_4SiN_{10}$by quantum methods. SCF GIAO Magnetic shielding tensors (ppm) consisting of an isotropic shielding tensor (σ_{iso}) and an anisotropic shielding tensor (σ_{aniso}).

CLQ			B_4AlN_{10}–CLQ			B_4CN_{10}–CLQ			B_4SiN_{10}–CLQ		
Atom	**σ_{iso}**	**σ_{aniso}**	**Atom**	**σ_{iso}**	**σ_{aniso}**	**Atom**	**σ_{iso}**	**σ_{aniso}**	**Atom**	**σ_{iso}**	**σ_{aniso}**
C1	132.52	130.65	B1	96.71	82.91	B1	103.95	91.64	B1	69.65	66.87
C2	134.71	115.73	N2	259.30	626.11	N2	111.66	621.75	N2	211.97	928.02
C3	154.14	132.97	N3	58.49	79.64	N3	1655.31	2921.16	N3	890.97	2652.00
C4	133.90	120.89	B4	105.97	72.42	B4	99.38	130.29	B4	93.00	40.07
C5	129.01	112.43	B5	94.94	58.17	B5	111.94	44.71	B5	56.79	52.74
C6	121.43	90.28	B6	78.48	78.26	B6	111.96	63.24	B6	55.44	76.88
C7	135.35	119.43	N7	180.32	573.04	N7	268.02	362.56	N7	147.71	1114.40
C8	145.64	85.83	N8	79.95	253.36	N8	557.61	1335.78	N8	1417.29	2153.41
C9	124.85	112.78	N9	460.09	832.80	N9	601.87	1305.01	N9	588.36	4046.60
N10	76.90	440.22	N10	558.79	717.03	N10	877.08	1752.31	N10	575.52	2937.29
N11	236.30	37.80	N11	512.23	941.85	N11	1094.84	1854.46	N11	88.60	3677.85
C12	179.56	34.90	N12	283.32	712.10	N12	637.42	1166.30	N12	300.50	2936.03
C13	204.91	29.29	Al13	488.58	206.97	C13	99.65	87.81	Si13	670.58	157.49
C14	198.50	27.14	N14	28.48	599.67	N14	35.63	1510.04	N14	123.22	1007.9
C15	200.92	22.42	N15	21.33	591.87	N15	262.85	1199.51	N15	40.17	1170.06

The [B_4XN_{10}–CLQ (X=Al/C/Si)] complexes have reflected the significance of chemical shielding consisting of σ_{iso} and σ_{aniso} (ppm) for diverse elements of B, Al, C, Si, N, and Cl atoms in the active zones of the system, owing to the NMR curve (Table 1).

Furthermore, the ^{13}C–NMR considerations on the CLQ drug have identified the active zones of this compound, owing to unraveling the most electron-donor elements during CLQ drug adsorption onto B_4XN_{10}(X=Al/C/Si) complexes, which expose the major shift in tetramethylsilane (TMS) using quantum methods (Figure 3a–d).

The most alterations were declared for atoms of N11 in CLQ drug (Figure 3a), N11, Al60 in B_4AlN_{10}–CLQ (Figure 3b), N11, C60 in B_4CN_{10}–CLQ (Figure 3c), N11, Si60 in B_4SiN_{10}–CLQ (Figure 3d).

The progress of impressive DFT methods, including electronic correlation effects, has been shown to be a significant key in the field of shielding computations. By DFT theory, which scales as N^2 (N=number of electrons), it is feasible to compute shielding in molecular systems of practical interest, considering electronic correlation impacts. Furthermore, new DFT approaches with linear scaling are available, which will enable further development in the implementation of these techniques for computing magnetic shielding in large systems [37].

This skeleton, based on the theory, analyzes the solvent effects on the magnetic shielding. The actual computation of these impacts is quite puzzling, because any model that seeks to capture these interactions must estimate both the electromagnetic interactions produced by solvent molecules and their dynamic parameters.

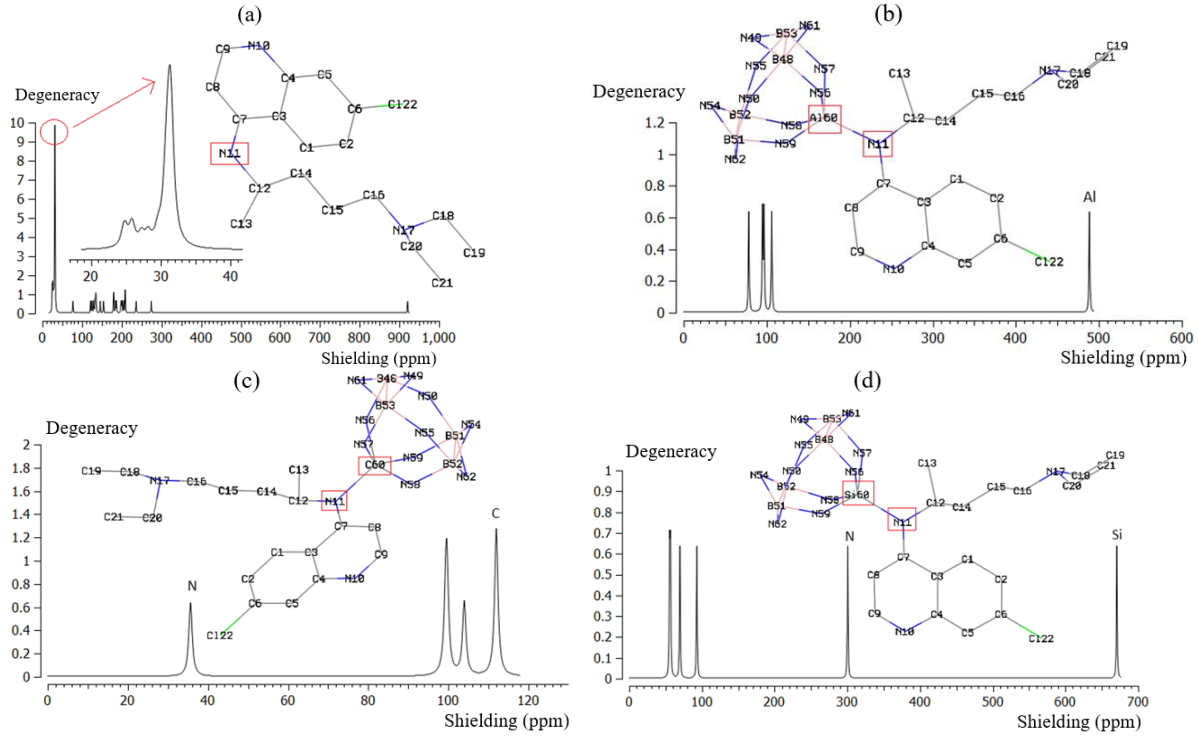

Figure 3. The NMR spectra for **(a)** CLQ drug; **(b)** B_4AlN_{10}–CLQ; **(c)** B_4CN_{10}–CLQ; **(d)** B_4SiN_{10}–CLQ.

3.3. NQR analysis.

Nuclear quadrupole resonance (NQR) spectra can provide precise structural and compositional information about active groups in biological reactions. It offers a high probability of identifying the quadrupole coupling constants and the associated charges, providing insight into the system's electronic structure. In fact, NQR spectra become visible, providing an intense tool for investigating diverse chemical influences in the solid phase of many nitrogen-containing substances. Analyzing the quadrupole coupling constants of nitrogen atoms permits an assessment of the electron density distribution on nitrogen nuclei and enables analysis of charge distribution in chemical bonding involving nitrogen atoms.

So, "nuclear quadrupole resonance" or "NQR" was evaluated for CLQ drug trapped by the surface of B_4XN_{10}(X=Al/C/Si) nanocages towards formation of [B_4XN_{10}–CLQ (X=Al/C/Si)] complexes based on the "nuclear quadrupole moment", and the "electric field gradient" or "EFG" [38].

As the "EFG" at the site of the nucleus in the CLQ drug is allocated by the valence electrons twisted in the particular attachment with close nuclei of B_4XN_{10}–CLQ(X=Al/C/Si) nanocages, the "NQR" frequency at which transitions occur is particular for [B_4XN_{10}–CLQ (X=Al/C/Si)] complexes (Table 2).

Table 2. The electric potential (E_p/a.u.) and Bader charge (Q/coulomb) through NQR calculation for functionalized elements of CLQ drug attached to B_4AlN_{10}, C–B_4N_{10}, and Si–B_4N_{10} nanocages using CAM-B3LYP/EPR-III,6-311+G(d,p) calculation.

CLQ			B_4AlN_{10}–CLQ			B_4CN_{10}–CLQ			B_4SiN_{10}–CLQ		
Atom	**Q**	**E_p**	**Atom**	**Q**	**E_p**	**Atom**	**Q**	**E_p**	**Atom**	**Q**	**E_p**
C1	0.01	–14.54	B1	–0.42	–11.30	B1	0.29	–11.27	B1	0.33	–11.26
C2	0.00	–14.54	N2	0.32	–18.14	N2	–0.15	–18.09	N2	–0.16	–18.11
C3	–0.04	–14.53	N3	–1.49	–18.12	N3	–0.13	–18.07	N3	–0.16	–18.10
C4	0.09	–14.51	B4	–0.37	–11.30	B4	0.29	–11.26	B4	0.33	–11.27
C5	0.04	–14.55	B5	–0.54	–11.30	B5	0.30	–11.28	B5	0.33	–11.26
C6	0.00	–14.50	B6	–0.26	–11.28	B6	0.29	–11.27	B6	0.33	–11.26

CLQ			B_4AlN_{10}–CLQ			B_4CN_{10}–CLQ			B_4SiN_{10}–CLQ		
Atom	**Q**	**E_p**	**Atom**	**Q**	**E_p**	**Atom**	**Q**	**E_p**	**Atom**	**Q**	**E_p**
C7	0.10	–14.47	N7	0.58	–18.14	N7	–0.15	–18.09	N7	–0.16	–18.12
C8	0.04	–14.57	N8	1.57	–18.13	N8	–0.13	–18.08	N8	–0.15	–18.09
C9	0.10	–14.53	N9	0.47	–18.20	N9	–0.10	–18.08	N9	–0.33	–18.18
N10	–0.28	–18.14	N10	–0.24	–18.20	N10	–0.10	–18.09	N10	–0.33	–18.17
N11	–0.07	–18.01	N11	–0.02	–18.18	N11	–0.09	–18.08	N11	–0.31	–18.16
C12	0.12	–14.46	N12	0.20	–18.18	N12	–0.10	–18.07	N12	–0.32	–18.15
C13	0.02	–14.52	Al13	–0.00	–43.70	C13	0.11	–14.53	Si13	0.96	–48.39
C14	0.02	–14.52	N14	0.73	–18.12	N14	–0.14	–18.08	N14	–0.18	–18.12
C15	0.01	–14.52	N15	0.46	–18.13	N15	–0.14	–18.08	N15	–0.18	–18.12

Furthermore, in Figure 4 (a–d), the electric potential versus Bader charge of nuclear quadrupole resonance for some atoms in the attachment of CLQ drug onto B_4XN_{10}(X=Al/C/Si) nanocages was measured by the theoretical method.

In Figure 4(a), the fluctuation of the charge distribution for all atoms in the CLQ drug was exhibited to understand which atoms have a more electron-donating tendency in the attachment to the B_4XN_{10}–CLQ (X=Al/C/Si) complexes.

On the other hand, the N atom in the CLQ drug acts as an electron donor, with a high-energy orbital containing one or more electrons. So, in B_4XN_{10}(X=Al/C/Si) complexes, the elements of Al, C, and Si can be considered as the electron acceptors, which have a low-energy orbital with one or more vacancies (Figure 4b, c, d).

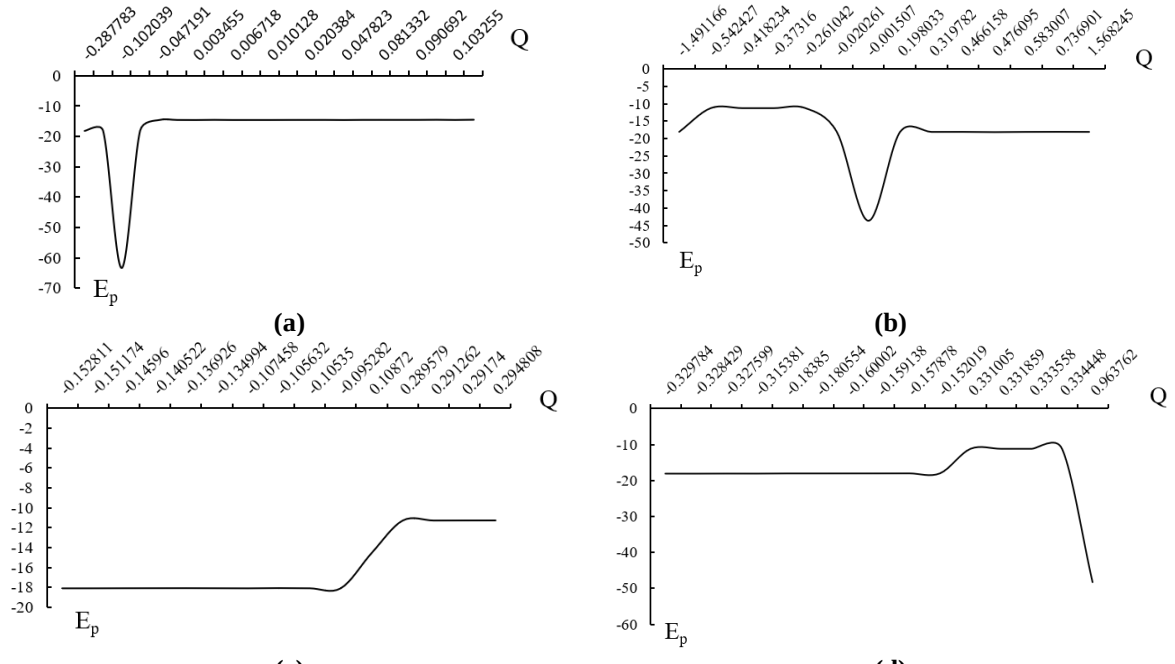

Figure 4. The amounts of electric potential (E_p/a.u.) versus Bader charge (Q/coulomb) through NQR calculation for **(a)** CLQ drug; **(b)** B_4AlN_{10}–CLQ; **(c)** B_4CN_{10}–CLQ; **(d)** B_4SiN_{10}–CLQ.

In fact, the influence of the linkage between N11 in the CLQ drug (Figure 4a) and Al60, C60, and Si60 in B_4AlN_{10}–CLQ (Figure 4b), B_4CN_{10}–CLQ (Figure 4c), and B_4SiN_{10}–CLQ (Figure 4d) complexes, respectively, during adsorbing CLQ is indicated by the achieved data of E_p from NQR spectroscopy. The competence of B_4XN_{10}(X=Al/C/Si) complexes for sensing CLQ is determined by their selectivity and sensitivity, which can indicate the yield of these materials as the engaged detectors.

3.4. Spectroscopy of IR.

The spectroscopy of infrared (IR) through some computations was completed for the CLQ drug (Figure 5a) attached to B_4XN_{10}(X=Al/C/Si) complexes by the DFT approach to catch a more stable system, accompanied by thermodynamic attributes. Therefore, several complexes containing B_4AlN_{10}–CLQ (Figure5b), B_4CN_{10}–CLQ (Figure 5c), and B_4SiN_{10}–CLQ (Figure 5d) have been simulated.

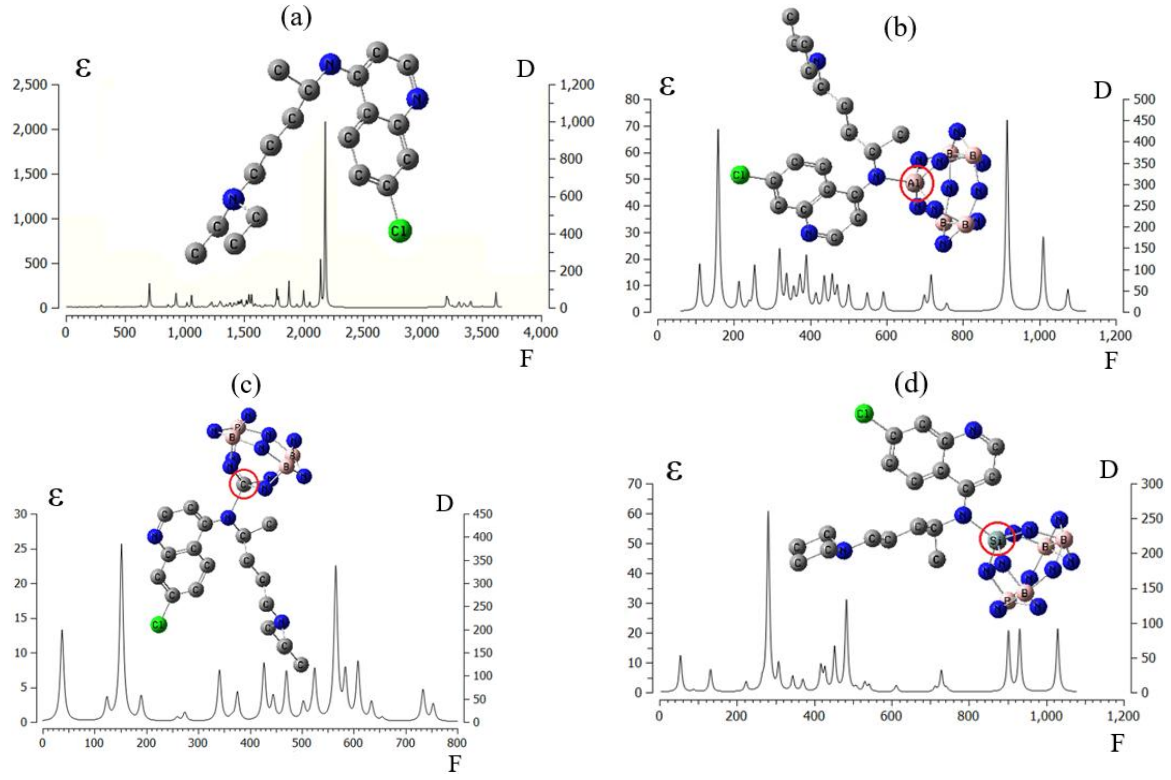

Figure5. The frequencies (F, cm^{-1}) of IR spectra for **(a)** CLQ drug; **(b)** B_4AlN_{10}–CLQ; **(c)** B_4CN_{10}–CLQ; **(d)** B_4SiN_{10}–CLQ.

ε ($M^{-1}cm^{-1}$ or $Lmol^{-1}cm^{-1}$) is the absorbance unit, and D (10^{-4} esu^2 cm^2) is the dipole strength via the esu or electrostatic unit, which is a unit of charge in the cgs (centimeter-gram-second) system.

The curve in Figure 5 (a) shows the frequency limitation across 500–3500 cm^{-1} for the CLQ drug with a sharp peak around 2183.43 cm^{-1}. Figure 5 (b) shows the frequency range between 100–1500 cm^{-1} for B_4AlN_{10}–CLQ with two sharp peaks around 158.81 and 915.64 cm^{-1}. Figure 5 (c) indicates the fluctuation of frequency between 50–750 cm^{-1} for B_4CN_{10}–CLQ with the sharp peaks around 37.34, 152.01, and 565.57 cm^{-1}. Figure 5 (d) shows the fluctuation of frequency between 100–1100 cm^{-1} for B_4SiN_{10}–CLQ with sharp peaks around 281.19, 483.33, 902.26, 931.18, and 1029.57 cm^{-1}.

The outlook of Figure 5 (a–d) provides evidence for different frequencies of [B_4XN_{10}–CLQ(X=Al/C/Si)] complexes, which indicate the active sites in the CLQ drug and functionalized atoms in B_4XN_{10}(X=Al/C/Si) that can transfer the charge of electrons in polar CLQ into the B_4XN_{10}(X=Al/C/Si) complexes.

Furthermore, Table 3, through the thermodynamic specifications, concluded that B_4XN_{10}(X=Al/C/Si), due to the adsorption of CLQ drug, might be a more efficient sensor for a drug delivery system.

Table 3. The thermodynamic characters thermal energy(ΔE°), thermal enthalpy (ΔH°), Gibbs free energy (ΔG°), entropy (S°), and dipole moment of CLQ drug, B_4AlN_{10}–CLQ, B_4CN_{10}–CLQ, B_4SiN_{10}–CLQ, using CAM-B3LYP/6-311+G (d, p), LANL2DZ calculation.

Compound	$\Delta E^o \times 10^{-4}$ (kcal/mol)	$\Delta H^o \times 10^{-4}$ (kcal/mol)	$\Delta G^o \times 10^{-4}$ (kcal/mol)	S^o (cal/K.mol)	Dipole moment (Debye)
CLQ drug	–821.875	–821.875	–821.913	129.091	5.8364
B_4AlN_{10}–CLQ	–55.0351	–55.0350	–55.0379	98.176	3.4260
B_4CN_{10}–CLQ	–42.3537	–42.3536	–42.3566	99.093	1.4160
B_4SiN_{10}–CLQ	–57.9539	–57.9538	–57.9568	99.252	1.2968

It is remarkable that polarization functions in the practical basis set in the enumerations indicate notable progress in quantum-theoretical techniques. The outcomes of the mentioned perceptions strongly suggest that CLQ is associated with the X–B_4N_{10} (X=Al/C/Si) complex, which is influenced by a mutation in the ambient polarization. It can be observed that an increase in the dielectric constant enhances the efficacy and stability of this medication for treating COVID-19.

The adsorption process of CLQ drug on the surface of functionalized B_4N_{10} by Al, C, and Si elements is affirmed by the ΔG_R^o quantity:

$$\Delta G_R^o = \Delta G^o_{B4XN10-CLQ} - \left(\Delta G^o_{CLQ-adsorbed} + \Delta G^o_{B4XN10}\right); X= Al, C, Si \quad (1)$$

As seen in Table 3, all accounted ΔG^o amounts of B_4AlN_{10}–CLQ, B_4CN_{10}–CLQ, and B_4SiN_{10}–CLQ are close, which can demonstrate an appropriate potential of these functionalized nanocages for CLQ drug adsorption as a drug delivery technique (Table 3).

4. Conclusions

A drug carrier or drug vehicle is a substance used in the process of delivering medicine. It helps make the drug more targeted, effective, and safer when it's given to a patient. These carriers are mainly used to manage how and when the drug is released into the body. In this work, the effect of the CLQ drug on the treatment of COVID-19 has been studied owing to its attachment to the B_4XN_{10} (X=Al/C/Si) complex surrounded by a periodic box of H_2O as the drug delivery technique. CLQ drug has motivated scientists to investigate the clinical therapy of viral coronavirus malady (COVID-19) using linkage to the B_4N_{10}, which can engage an impressive drug delivery approach due to PDOS, NMR, IR, and NQR data analysis on the optimized structure extracted from DFT measurements. It can be stated that the doped nanocages, particularly B_4AlN_{10}–CLQ, B_4CN_{10}–CLQ, and B_4SiN_{10}–CLQ, show better chloroquine delivery compared to the original nanocage because they have better thermodynamic properties, stronger magnetic and electronic features, and higher reactivity.

Institutional Review Board Statement

Not applicable.

Informed Consent Statement

Not applicable.

Data Availability Statement

Data supporting the findings of this study are available upon reasonable request from the corresponding author.

Funding

This research received no funding.

Acknowledgments

The author is grateful to Kastamonu University for supporting the successful completion of this paper and the research.

Conflict of Interest

The author declares no conflict of interest.

References

1. Angius, F.; Puxeddu, S.; Zaimi, S.; Canton, S.; Nematollahzadeh, S.; Pibiri, A.; Delogu, I.; Alvisi, G.; Moi, M.L.; Manzin, A. SARS-CoV-2 Evolution: Implications for Diagnosis, Treatment, Vaccine Effectiveness and Development. *Vaccines* **2025**, *13*, 17, https://doi.org/10.3390/vaccines13010017.
2. Anand, A.; Vialard, F.; Esmail, A.; Ahmad Khan, F.; O'Byrne, P.; Routy, J.-P.; Dheda, K.; Pant Pai, N. Self-tests for COVID-19: What is the evidence? A living systematic review and meta-analysis (2020–2023). *PLOS Global Public Health* **2024**, *4*, e0002336, https://doi.org/10.1371/journal.pgph.0002336.
3. Subong, B.J.J.; Forteza, I.L. SARS-CoV-2 Replication Revisited: Molecular Insights and Current and Emerging Antiviral Strategies. *COVID* **2025**, *5*, 85, https://doi.org/10.3390/covid5060085.
4. Bhatia, A.; Preiss, A.J.; Xiao, X.; Brannock, M.D.; Alexander, G.C.; Chew, R.F.; Davis, H.; Fitzgerald, M.; Hill, E.; Kelly, E.P.; Mehta, H.B.; Madlock-Brown, C.; Wilkins, K.J.; Chute, C.G.; Haendel, M.; Moffitt, R.; Pfaff, E.R.; the, N.C.C. Effect of nirmatrelvir/ritonavir (Paxlovid) on hospitalization among adults with COVID-19: An electronic health record-based target trial emulation from N3C. *PLOS Med.* **2025**, *22*, e1004493, https://doi.org/10.1371/journal.pmed.1004493.
5. Ciftci, H.; Sabirli, R.; Koseler, A.; Canacik, O.; Karsli, E.; Ercin, D.; Tutuncu, E.E.; Kurt, O. Serum Hypoxia-Inducible Factor 1 Alpha Levels Decrease in Patients with COVID-19: A Case-Control Study. *COVID* **2026**, *6*, 89, https://doi.org/10.3390/covid6050089.
6. Ivanov, K.I.; Yang, H.; Sun, R.; Li, C.; Guo, D. The emerging role of SARS-CoV-2 nonstructural protein 1 (nsp1) in epigenetic regulation of host gene expression. *FEMS Microbiol. Rev.* **2024**, *48*, fuae023, https://doi.org/10.1093/femsre/fuae023.
7. Batool, S.; Chokkakula, S.; Jeong, J.H.; Baek, Y.H.; Song, M.-S. SARS-CoV-2 drug resistance and therapeutic approaches. *Heliyon* **2025**, *11*, e41980, https://doi.org/10.1016/j.heliyon.2025.e41980.
8. Alhamlan, F.S.; Al-Qahtani, A.A. SARS-CoV-2 Variants: Genetic Insights, Epidemiological Tracking, and Implications for Vaccine Strategies. *Int. J. Mol. Sci.* **2025**, *26*, 1263, https://doi.org/10.3390/ijms26031263.
9. Rashid, S.A.; Anasir, M.I.; Arsad, F.S.; Shahrir, N.F.; Kamel, K.A.; Rajendiran, S.; Khairul Hasni, N.A.; Mazeli, M.I.; Veloo, Y.; Syed Abu Thahir, S.; Wan Mahiyuddin, W.R.; Chin, K.B.; Mohd Aris, A.; Zainudin, R.; Shaharudin, R.; Nazakat, R. Influence of Sampling Strategies and Disease Prevalence on SARS-CoV-2 Detection Dynamics in Wastewater Surveillance. *Viruses* **2026**, *18*, 583, https://doi.org/10.3390/v18050583.
10. Barušić, Z.; Bodulić, K.; Zember, S.; Laškaj, R.; Čivljak, R.; Puljiz, I.; Kurolt, I.-C.; Šafranko, Ž.M.; Krajinović, L.C.; Karić, P.S.; Markotić, A. Prognostic Value of Biomarkers in COVID-19: Associations with Disease Severity, Viral Variants, and Comorbidities—A Retrospective Observational Single-Center Cohort Study. *Life* **2025**, *15*, 634, https://doi.org/10.3390/life15040634.

11. Stoichita, A.; Mahler, B.; Vlasceanu, S.; Parliteanu, O.; Dragomir, J.A.; Balteanu, M.; Radu, A.D.; Teleaga, C.; Baiceanu, D.; Panciu, T.C.; Madalina, M.; Ibraim, E.; Ciupan, M.M.; Iliesiu Mihaela, A. Post-COVID-19 Cardiovascular Complications: An Updated Systematic Review. *J. Respir.* **2026**, *6*, 4, https://doi.org/10.3390/jor6010004.
12. Woodall, M.; Ellis, S.; Zhang, S.; Kembou-Ringert, J.; Kite, K.-A.; Buggiotti, L.; Jacobs Amy, I.; Agyeman Akosua, A.; Masonou, T.; Palor, M.; McHugh Timothy, D.; Breuer, J.; Standing Joseph, F.; Smith Claire, M. Efficient *in vitro* assay for evaluating drug efficacy and synergy against emerging SARS-CoV-2 strains. *Antimicrob. Agents Chemother.* **2024**, *69*, e01233-01224, https://doi.org/10.1128/aac.01233-24.
13. Gu, X.; Zheng, M.; Gao, Y.; Lin, S.; Zhang, X.; Chen, C.; Zhu, H.; Sun, W.; Zhang, Y. Overview of host-directed antiviral targets for future research and drug development. *Acta Pharm. Sin. B* **2025**, *15*, 1723-1751, https://doi.org/10.1016/j.apsb.2025.03.011.
14. Ureshino, R.P.; Sousa, L.A.d.; Oliveira, R.B.; Saullo, G.A.; Zonaro, P.H.; Newson, L.; Prado, C.M.; Stilhano, R.S. Excitotoxicity and Neurological Post-COVID-19 Syndrome: Exploring Possible Connections of Pathophysiological Mechanisms. *COVID* **2026**, *6*, 85, https://doi.org/10.3390/covid6050085.
15. Chikhoune, L.; Poggi, C.; Moreau, J.; Dubucquoi, S.; Hachulla, E.; Collet, A.; Launay, D. JAK inhibitors (JAKi): Mechanisms of action and perspectives in systemic and autoimmune diseases. *Rev. Med. Interne* **2025**, *46*, 89-106, https://doi.org/10.1016/j.revmed.2024.10.452.
16. Jiang, Q.; Yang, S.; He, S.; Li, F. AI drug discovery tools and analysis technology: New methods aid in studying the compatibility of Traditional Chinese Medicine. *Pharmacol. Res. - Mod. Chin. Med.* **2025**, *14*, 100566, https://doi.org/10.1016/j.prmcm.2024.100566.
17. Kubryń, N.; Fijałkowski, Ł.; Nowaczyk, J.; Jamil, A.; Nowaczyk, A. PROTAC Technology as a New Tool for Modern Pharmacotherapy. *Molecules* **2025**, *30*, 2123, https://doi.org/10.3390/molecules30102123.
18. Keshav, V.; Scott, L.; Hans, L.; Stevens, W. Performance Evaluation of Instrument-Based SARS-CoV-2 Rapid Antigen Fluorescent Immunoassays for Point-of-Care Detection. *COVID* **2026**, *6*, 78, https://doi.org/10.3390/covid6050078.
19. Pan, B.; Mountford, S.J.; Kiso, M.; Anderson, D.E.; Papadakis, G.; Jarman, K.E.; Tilmanis, D.R.; Maher, B.; Tran, T.; Shortt, J.; Yamayoshi, S.; Kawaoka, Y.; Thompson, P.E.; Greenall, S.A.; Warner, N. Targeted protein degraders of SARS-CoV-2 Mpro are more active than enzymatic inhibition alone with activity against nirmatrelvir resistant virus. *Commun. Med.* **2025**, *5*, 140, https://doi.org/10.1038/s43856-025-00863-1.
20. Schreiber, A.; Ludwig, S. Host-targeted antivirals against SARS-CoV-2 in clinical development - Prospect or disappointment? *Antivir. Res.* **2025**, *235*, 106101, https://doi.org/10.1016/j.antiviral.2025.106101.
21. Fu, C.; Chen, Q. The future of pharmaceuticals: Artificial intelligence in drug discovery and development. *J. Pharm. Anal.* **2025**, *15*, 101248, https://doi.org/10.1016/j.jpha.2025.101248.
22. Silva Rívolli, A.C.; Lima, I.A.d.S.; Reis, C.C.C.d.; Antonio, Í.R.; Samed, M.M.A. Logistical Performance of a COVID-19 Vaccination Campaign in a Decentralized Health System. *COVID* **2026**, *6*, 73, https://doi.org/10.3390/covid6050073.
23. Mollaamin, F.; Monajjemi, M. Application of DFT and TD-DFT on Langmuir Adsorption of Nitrogen and Sulfur Heterocycle Dopants on an Aluminum Surface Decorated with Magnesium and Silicon. *Computation* **2023**, *11*, 108, https://doi.org/10.3390/computation11060108.
24. Mollaamin, F. Computational Methods in the Drug Delivery of Carbon Nanocarriers onto Several Compounds in Sarraceniaceae Medicinal Plant as Monkeypox Therapy. *Computation* **2023**, *11*, 84, https://doi.org/10.3390/computation11040084.
25. Shahriari, S.; Monajjemi, M.; Mollaamin, F. DETERMINATION OF PROTEINS SPECIFICATION WITH SARS- COVID-19 BASED LIGAND DESIGNING. *J. Chil. Chem. Soc.* **2022**, *67*, 5468–5476, https://doi.org/10.4067/S0717-97072022000205468.
26. Saripilli, R.; Sharma, D.K. Nanotechnology-based drug delivery system for the diagnosis and treatment of ovarian cancer. *Discov. Oncol.* **2025**, *16*, 422, https://doi.org/10.1007/s12672-025-02062-9.
27. Wehbe, R.; Khoshman, N.; Ousseily, Z.; Al-Tameemi, S.A.; Majzoub, R.E.; Najar, M.; Merimi, M.; Fayyad-Kazan, H.; Badran, B.; Fayyad-Kazan, M. Emerging SARS-CoV-2 variants: genomic shifts,

immune evasion, and therapeutic perspectives. *Mol. Biol. Rep.* **2025**, *52*, 886, https://doi.org/10.1007/s11033-025-11009-w.
28. Guan, H.; Sun, H.; Zhao, X. Application of Density Functional Theory to Molecular Engineering of Pharmaceutical Formulations. *Int. J. Mol. Sci.* **2025**, *26*, 3262, https://doi.org/10.3390/ijms26073262.
29. Azum, N.; Rub, M.A.; Chani, M.T.S.; Alzahrani, K.A.; Asad, M.; Kamal, T. Mixed Micellization and Density Functional Theory (DFT) Studies on the Molecular Interactions between Gemini and Nonionic Surfactants. *J. Oleo Sci.* **2025**, *74*, 47-59, https://doi.org/10.5650/jos.ess24095.
30. Becke, A.D. Density-functional exchange-energy approximation with correct asymptotic behavior. *Phys. Rev. A.* **1988**, *38*, 3098, https://doi.org/10.1103/PhysRevA.38.3098.
31. Lee, C.; Yang, W.; Parr, R.G. Development of the Colle-Salvetti correlation-energy formula into a functional of the electron density. *Phys. Rev. B* **1988**, *37*, 785, https://doi.org/10.1103/PhysRevB.37.785.
32. Onsager, L. Electric Moments of Molecules in Liquids. *J. Am. Chem. Soc*. **1936**, *58*, 1486–1493, https://doi.org/10.1021/ja01299a050.
33. Cramer, C.J.; Truhlar, D.G. PM3-SM3: A general parameterization for including aqueous solvation effects in the PM3 molecular orbital model. *J. Comput. Chem.* **1992**, *13*, 1089-1097, https://doi.org/10.1002/jcc.540130907.
34. Kazachenko, A.S.; Issaoui, N. Advancing the Frontiers: Contemporary Achievements and Future Directions in Density Functional Theory Calculations. *Molecules* **2026**, *31*, 676, https://doi.org/10.3390/molecules31040676.
35. Amić, A.; Mastiľák Cagardová, D.; Milanović, Ž. Theoretical Study of Antioxidant and Prooxidant Potency of Protocatechuic Aldehyde. *Int. J. Mol. Sci.* **2025**, *26*, 404, https://doi.org/10.3390/ijms26010404.
36. Frisch, M.J.; Trucks, G.W.; Schlegel, H.B.; Scuseria, G.E.; Robb, M.A.; Cheeseman, J.R.; Scalmani, G.; Barone, V.; Petersson, G.A.; Nakatsuji, H.; Li, X.; Caricato, M.; Marenich, A.V.; Bloino, J.; Janesko, B.G.; Gomperts, R.; Mennucci, B.; Hratchian, H.P.; Ortiz, J. V.; Izmaylov, A. F.; Sonnenberg, J.L.; Williams-Young, D.; Ding, F.; Lipparini, F.; Egidi, F.; Goings, J.; Peng, B.; Petrone, A.; Henderson, T.; Ranasinghe, D.; Zakrzewski, V.G.; Gao, J.; Rega, N.; Zheng, G.; Liang, W.; Hada, M.; Ehara, M.; Toyota, K.; Fukuda, R.; Hasegawa, J.; Ishida, M.; Nakajima, T.; Honda, Y.; Kitao, O.; Nakai, H.; Vreven, T.; Throssell, K.; Montgomery, J.A., Jr.; Peralta, J.E.; Ogliaro, F.; Bearpark, M.J.; Heyd, J.J.; Brothers, E.N.; Kudin, K.N.; Staroverov, V.N.; Keith, T.A.; Kobayashi, R.; Normand, J.; Raghavachari, K.; Rendell, A.P.; Burant, J.C.; Iyengar, S.S.; Tomasi, J.; Cossi, M.; Millam, J.M.; Klene, M.; Adamo, C.; Cammi, R.; Ochterski, J.W.; Martin, R.L.; Morokuma, K.; Farkas, O.; Foresman, J.B.; Fox, D.J. Gaussian 16, Revision C.01, Gaussian, Inc., Wallingford CT, **2016**.
37. Gerothanassis, I.P.; Kupka, T. New Insights into Nuclear Magnetic Resonance (NMR) Spectroscopy. *Molecules* **2025**, *30*, 1500, https://doi.org/10.3390/molecules30071500.
38. Mollaamin, F. Features of Parametric Point Nuclear Magnetic Resonance of Metals Implantation on Boron Nitride Nanotube by Density Functional Theory/Electron Paramagnetic Resonance. *J. Comput. Theor. Nanosci.* **2014**, *11*, 2393–2398, https://doi.org/10.1166/jctn.2014.3653.

Publisher's Note & Disclaimer